NANO LETTERS
Letter
Cite This: Nano Lett. 2018, 18, 7268−7274
pubs.acs.org/NanoLett

Light-Guided Motility of a Minimal Synthetic Cell

Solveig M. Bartelt,[†] Jan Steinkühler,[‡] Rumiana Dimova,[‡] and Seraphine V. Wegner*[,†]

[†]Max Planck Institute for Polymer Research, Ackermannweg 10, 55128 Mainz, Germany
[‡]Theory and Bio-Systems, Max Planck Institute of Colloids and Interfaces, Science Park Golm, 14424 Potsdam, Germany

Supporting Information

ABSTRACT: Cell motility is an important but complex process; as cells move, new adhesions form at the front and adhesions disassemble at the back. To replicate this dynamic and spatiotemporally controlled asymmetry of adhesions and achieve motility in a minimal synthetic cell, we controlled the adhesion of a model giant unilamellar vesicle (GUV) to the substrate with light. For this purpose, we immobilized the proteins iLID and Micro, which interact under blue light and dissociate from each other in the dark, on a substrate and a GUV, respectively. Under blue light, the protein interaction leads to adhesion of the vesicle to the substrate, which is reversible in the dark. The high spatiotemporal control provided by light, allowed partly illuminating the GUV and generating an asymmetry in adhesions. Consequently, the GUV moves into the illuminated area, a process that can be repeated over multiple cycles. Thus, our system reproduces the dynamic spatiotemporal distribution of adhesions and establishes mimetic motility of a synthetic cell.

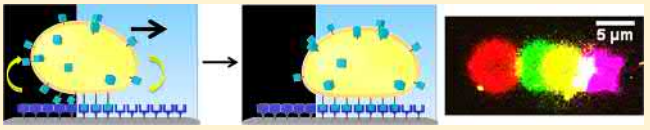

KEYWORDS: *Motility, optogenetics, GUV adhesion, synthetic cell, photoswitchable*

Motility is a key feature of living cells and is at the core of complex life processes including immune response, development, and the progression of diseases.[1] Mammalian cell motility on a two-dimensional (2D) substrate is a complex multistep event that requires four synchronized steps: (1) formation of membrane protrusions, (2) new adhesions to the substrate at the leading edge, (3) contraction of the cell body, and (4) detachment at the trailing edge.[2] To orchestrate these processes the cell relies on a complex molecular machinery including the actin cytoskeleton to form protrusions, integrins, which mediate adhesion to the substrate, myosin-dependent contractions, and a multitude of other regulatory proteins to coordinate different steps. An additional layer of complexity is that in a moving cell the symmetry between the back and the front is broken and different events, which span different time and length scales, have to be spatiotemporally controlled and synchronized (Figure 1A).

To understand the underlying complexity of cell motility, minimal synthetic cells provide simplified models and give mechanistic insight into how different machinery contributes to the process.[3] Toward this goal different machinery required for cell motility to form cell protrusions, contraction and adhesion have been introduced in GUVs (giant unilamellar vesicles), which are frequently used as a cell-like compartment.[4] In GUVs, the polymerization of actin in the presence of motor proteins leads to the deformation of the vesicle, formation of membrane protrusions, and oscillatory motion of the vesicles.[5,6] Adding myosin and coupling the actomyosin network to the membrane generates tension and results in symmetry breaking during the contraction of the network but does not lead to GUV movement. Furthermore, the cell adhesion receptor, integrin, has been functionally incorporated into GUVs and can prompt adhesion to substrates functionalized with the adhesion peptide RGD and extracellular matrix proteins.[7−11] Likewise, other interactions such as biotin−streptavidin,[12] E-cadherin,[13] lectin-sugar[14] and electrostatic interactions[15,16] were used to understand GUV adhesion to substrates. Despite all these studies, which provide great molecular insight into key players in cell motility, none of them have achieved the ultimate goal of replicating cell motility.

Part of the challenge in mimicking cell motility in a minimal synthetic cell is that in a migrating cell there is an asymmetry in terms of adhesion between the leading and the trailing edge. More and new adhesions form at the front to generate high traction forces coupled to the actin network and fewer adhesions at the back, which disassemble, enable the detachment, and retraction of the cell rear. Overall this asymmetry in adhesions is dynamically maintained and results in a directional cell movement. Replicating this dynamic spatiotemporal distribution of adhesions in a minimal synthetic cell requires a trigger that induces asymmetry in adhesions between the front and rear of a GUV and hinders the system to reach an equilibrium state. Such a trigger must provide spatial control at the sub GUV scale (typical diameter about 20 μm) and temporal control at a time scale that is relevant for a migrating cell (typical speed between 0.1 to 4 μm/min[17]). In addition, like in a cell these triggered adhesions must be reversible and have matching formation and reversion kinetics so that the trailing edge can detach as new adhesion are formed in the front. Current synthetic cell models based on integrins and synthetic interactions neither provide such spatiotemporal control nor the required reversibility and dynamics.

Received: August 27, 2018
Revised: October 12, 2018
Published: October 16, 2018

DOI: 10.1021/acs.nanolett.8b03469
Nano Lett. 2018, 18, 7268−7274

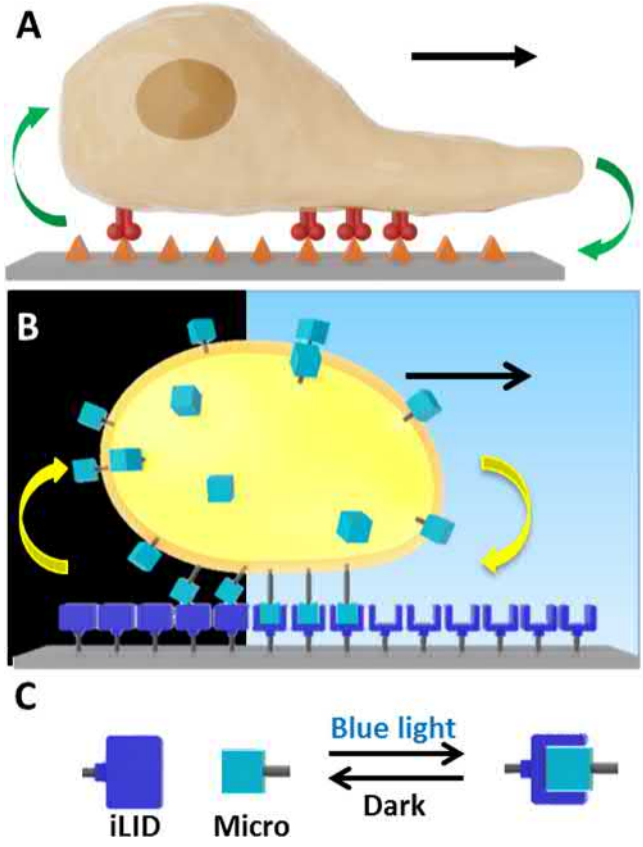

Figure 1. Cell vs GUV motility. (A) Simplified scheme of cell motility. Cell motility requires new adhesions to form at the leading edge, whereas adhesions have to disassemble at the trailing edge for the cell to move forward. The adhesion receptor integrin, is shown in red and the adhesion motif on the substrate in orange. (B) The light-controlled adhesion of a GUV allows to spatiotemporally control adhesions by partially illuminating the GUV. This mimics the dynamic asymmetry of adhesions in a minimal synthetic cell and leads to movement of the GUV. (C) The proteins iLID and Micro interact under blue light and dissociate in the dark.

To reproduce cell motility in a minimal synthetic cell and create dynamic asymmetry in adhesions, we established reversible GUV adhesions with high spatiotemporal control and matching on/off dynamics. For this aim, we propose to control the adhesion of GUVs to a substrate with visible light by using photoswitchable protein interactions as adhesion mediators (Figure 1B). Photoswitchable proteins provide reversible remote control at micrometer spatial resolution and down to second time scales with visible light.[18,19] Some photoswitchable protein interactions have already been used to control the interactions of mammalian and bacterial cells with substrates using light.[20,21] A critical parameter in selecting the photoswitchable protein interaction is that it has comparable on and off switching dynamics, so that the front and the rear of the GUV move at the same speed. In particular, we picked the photoswitchable protein iLID (improved light-induced dimer protein, based on the LOV2 domain), which binds to the protein Micro under blue light and dissociates from it in the dark (Figure 1C).[22] Our choice for this couple is based on the fact that the interaction between iLID and Micro reverses quickly in the dark within seconds to minutes, which matches the fast photoactivation with blue light. Other photoswitchable protein interactions like those between the PhyB and PIF6 under red light as well as CRY2 and CIBN or nMagHigh and pMagHigh under blue light activate much faster with light than they reverse in the dark.[20,21] The rapid deactivation of the PhyB/PIF interaction is possible with far-red light but is technically more complex as it would require the coillumination with a second far-red light source.

As the first step to establish photoswitchable adhesions, we immobilized His-tagged iLID as the adhesion ligand onto a polyethylene glycol (PEG)-coated glass substrate with Ni^{2+}-NTA end groups (Ni^{2+}-NTA end groups about 40 pmol/cm^2)[23] through the His-tag-Ni^{2+}-NTA interaction and His-tagged Micro as the adhesion receptor onto deflated GUVs (POPC + 10 mol% POPG + 0.1 mol % DGS-Ni^{2+}-NTA, Ni^{2+}-NTA end groups ca. 0.25 pmol/cm^2) including a lipid with a Ni^{2+}-NTA headgroup (Figure 2A). The GUVs were osmotically deflated by partially evaporating the outer buffer, leading to excess membrane allowing for membrane fluctuations and various vesicle morphologies including spherical-cap-like adhering states.[24] In addition, the GUVs were loaded with a solution (100 mM sucrose) of higher density compared to that of their surrounding so that they sunk onto the substrate. The vesicles were labeled with a red-shifted fluorescent dye (1,1′-dioctadecyl-3,3,3′,3′-tetramethylindodicarbocyanine) to observe them with confocal microscopy in *x,z* direction without activating the photoswitchable protein interaction. In the dark, Micro functionalized GUVs settled on the iLID functionalized substrate but did not exhibit significant adhesion, that is, the GUVs were free to displace by diffusion and convection and the weak membrane-substrate interactions were also witnessed by thermal membrane undulations in the vicinity of the substrate (Figure 2B, t = 0 min). Only upon activation of the iLID−Micro interaction with blue light (Laser at 488 nm), the GUVs adhered strongly to the substrate, as observed from the deformation of the GUV expressed in an increase in adhesion area and suppression of optically resolvable membrane fluctuations in the adhesion segment (Figure 1B, t = 15 min, Supporting Information, Figure S1). This adhesion was reversible in the dark. After turning off the blue light, the adhesion area decreased approximately to the initial dark state (Figure 2B, t = 20 min). The adhesion of the GUVs could be turned on and off repeatedly over four blue light/dark cycles (Supporting Information, Figure S2). Additional control experiments showed that the GUVs do not adhere to the iLID-functionalized substrate in the dark over time or if the GUVs were not functionalized with Micro (Supporting Information, Figure S3). Similarly, GUVs also adhered light-dependently if the position of the iLID and Micro proteins are swapped, that is, immobilizing iLID on the GUV and Micro on the substrate (Supporting Information, Figure S4). Nonetheless, in all following experiments we immobilized the light-activated protein partner iLID on the PEG-coated glass substrate, so that iLID is not mobile and its spatially controlled photoactivation is not wiped out by diffusion in the GUV membrane.

When the membrane stiffness of the GUVs was increased by adding cholesterol, the light-triggered GUV deformation was less pronounced, showing only reduced formation of an adhered membrane segment (20 mol % cholesterol) or adhered membrane segments that were below the optical resolution (40 mol % cholesterol) (Supporting Information, Figure S5). Likewise, when the GUVs were not osmotically deflated, the light-dependent GUV adhesions only led to minor deformation of the GUV (Supporting Information, Figure S6).

DOI: 10.1021/acs.nanolett.8b03469
Nano Lett. 2018, 18, 7268−7274

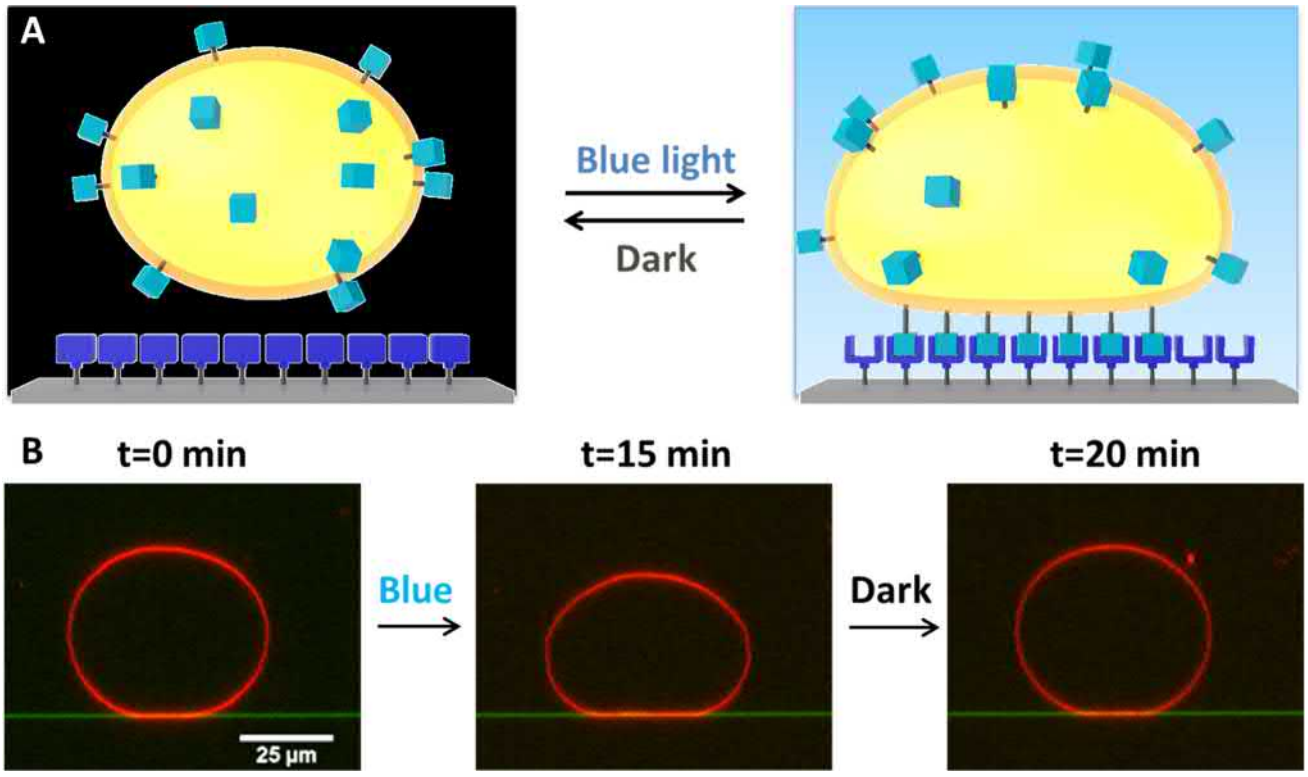

Figure 2. Light-dependent adhesion of a GUV to a substrate. (A) Light-dependent adhesion of a GUV decorated with Micro to a substrate functionalized with iLID. Upon light illumination the GUV adheres to the substrate and detaches in the dark. (B) Fluorescence microscopy images of a GUV over a time line being illuminated with blue light for 15 min adhered (compare first and second image). After further 5 min in the dark the GUV detached (last image). Micrographs represent (x,z) side-views. Red channel is membrane dye and green channel is the reflection of the 561 nm laser at the glass−water interface.

Hence, lower bending rigidity of the deflated GUVs is a critical requirement to observe light-dependent GUV deformation and membrane fluctuations to mimic the protrusions formed in migrating cell.

Kinetics of the light-induced adhesion and unbinding were quantified by time-resolved imaging and analysis of the GUV-substrate contact area (Figure 3A). The GUVs showed an increase of adhesion region to about double the size within the first 10 min of blue light illumination (Figure 3A, Light). Subsequently, when the GUVs were placed in the dark, the adhesion area of the GUVs decreased back to about its initial value within 5−6 min (Figure 3A Dark). However, the exact kinetics did vary between individual GUVs, presumably reflecting the complex relationship between membrane adhesion and iLID light activation, membrane dynamics, vesicle tension and size (Supporting Information, Figure S7). The fact that the adhesion under blue light and detachment in the dark take place at a similar and at minute time scale is important as the kinetics of attachment in the front and of detachment in the back of the GUV should match so that the cell can move in one piece. Notably, in a migrating cell adhesion and detachment also takes place on this time scale. When cells adhere, integrins enrich/cluster at the adhesion site and are depleted from other parts of the cell membrane. We used mOrange tagged Micro to observe whether Micro also enriched at the adhesion site upon photoactivation but could not detect significant Micro enrichment at the adhesion site (Supporting Information, Figure S8). It is also interesting that in some cases upon reversing GUV adhesion in the dark, excessive membrane shedding in the form of small vesicles from the GUVs is observed (Supporting Information, Figure S9). This observation supports the idea that upon light activation the excess membrane of the deflated GUVs contributes to the increase in adhesion area, whereas upon decrease in adhesion this membrane can spontaneously bud off. Yet, it should be noted that such loss of membrane over repeated light/dark cycles will be a limitation for motility over long distances. The budding may be an indication of a change in the membrane spontaneous curvature because of local asymmetry induced by protein interactions in the vicinity of the adhesion zone.[25]

For this study it was critical that there was a difference in binding strength in the dark and under blue light and that adhesion and detachment kinetics match, which led us to determine kinetic and thermodynamic parameters for the iLID and Micro interaction under blue light and in dark. In the QCM-D (quartz crystal microbalance with dissipation monitoring) studies, iLID was immobilized on a supported lipid bilayer (DOPC + 5 mol % DGS-NTA) formed on a SiO_2 crystal. Five mol % DGS-NTA was required in QCM-D measurements for the reliable detection of His-tagged iLID binding. Subsequently, increasing concentrations of Micro were passed over the QCM-D crystal either in the dark or under blue light illumination and both the binding and unbinding kinetics were monitored (Supporting Information, Figure S10). We observed that Micro binds to iLID both in the dark and under blue light, however the binding is more prominent under blue light. The analysis of the QCM-D curves showed that the K_d (dissociation constant) for the iLID−Micro interaction is 2.6 μM in the dark and 952 nM under

DOI: 10.1021/acs.nanolett.8b03469
Nano Lett. 2018, 18, 7268−7274

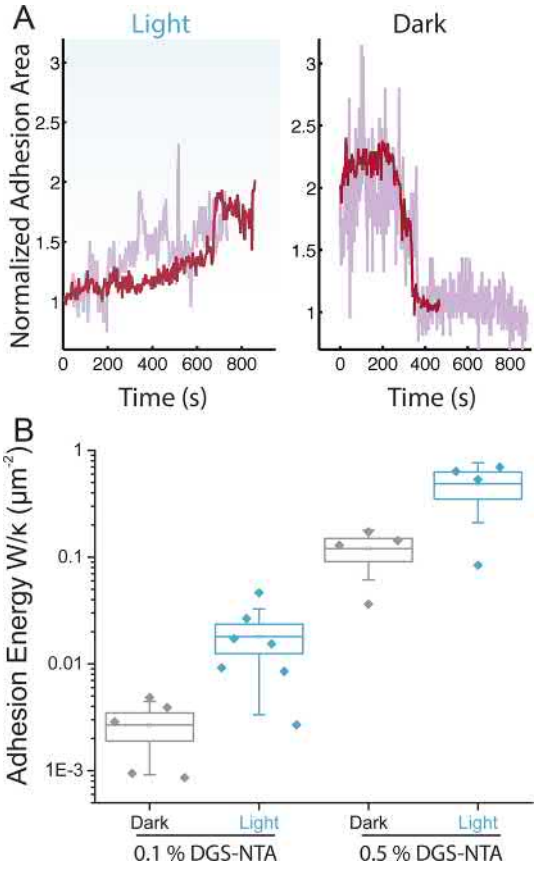

Figure 3. Quantification of adhesion. (A) Examples of time-dependent evolution of the normalized adhesion area versus time under blue light illumination and in the dark of two different GUVs (red and pink traces). Under blue light, an increase to about 1.8 times of the initial adhesion area was observed and subsequently in the dark the adhesion area decreased back to its initial value. Note that changes in adhesion area were related to adhesion energy, see eq 1 in SI. (B) Adhesion energies for GUVs functionalized with different Micro concentrations (0.1 mol % and 0.5 mol % DGS-NTA lipid for Micro immobilization) in the dark or under blue light. The adhesion energy W (rescaled by the GUV bending rigidity $\kappa \approx 20\ k_BT$[28]) for the 0.1 mol % DGS-NTA containing GUVs under blue light activation corresponds to about 0.4 $k_BT/\mu m^2$, which was used in the following light guiding experiments. All populations were found to be significantly different from each other ($p < 0.05$ Student t-test).

blue light, which equals a 2.7-fold increase in binding affinity under blue light (Supporting Information, Figure S11). Although a 2.7-fold difference in interactions seems small, it is notable that this difference is enough to trigger light-dependent adhesion of the GUVs. Further, these values are significantly different from the reported K_ds of 47 μM in the dark and 800 nM under blue light (58-fold change) of the proteins in solution,[22] showing that the immobilization of the iLID to a membrane affects the binding significantly. The k_{off} for the iLID−Micro interaction is similar in dark and under blue light ($k_{off,dark} = 8.5 \times 10^{-4}\ s^{-1}$, $k_{off,blue} = 1.1 \times 10^{-3}\ s^{-1}$) but the k_{on} increases significantly under blue light ($k_{on,dark} = 3.2 \times 10^2\ M^{-1}\ s^{-1}$, $k_{on,blue} = 1.2 \times 10^3\ M^{-1}\ s^{-1}$). These ranges of k_{off} and k_{on} are similar to those measured for integrin-extracellular protein binding (Supporting Information, Table S1).[26,27] This is an additional aspect in which the iLID-Micro interaction is similar to cell-matrix interactions of the cell in terms of dynamics but without coupling them to the intracellular machinery.

The light-dependent adhesion of the GUVs was quantified by measurement of the membrane-substrate adhesion energy, which depends on the concentration of Micro on the GUV and number of light activated iLID on the substrate. In turn, the contact area and global shape of adhering GUVs depends on the adhesion energy, the membrane tension (or excess area) and the bending rigidity.[24] The osmotically deflated GUVs exhibited varying membrane tension and, as expected, areas of the adhered membrane segments were found to be heterogeneous within a population. To estimate the interaction energy between the GUV and substrate, the GUV area and volume were estimated from three-dimensional reconstructions obtained by confocal microscopy.[16,29] In the dark, when Micro surface concentration was kept low (0.1 mol % DGS-NTA lipid for anchoring His-tagged Micro to the GUV), the adhesion energies between GUV and substrate were found to be smaller than $10^{-1}\ k_BT/\mu m^{-2}$ and GUVs were essentially unbound (Figure 3B left). In contrast, light activation increased the adhesion energy to about 0.4 $k_BT/\mu m^{-2}$. The change of adhesion energy between the dark and blue light activated state is about 6-fold and, interestingly, exceeds the change in iLID-Micro binding affinity of 2.7 fold. Presumably, this effect is at least partly due to the cooperative and nonlinear dependence between membrane adhesion energy and receptor−ligand complex formation through suppression of membrane fluctuations.[30,31] As expected, an increase in Micro surface concentration (0.5 mol % DGS-NTA lipid, Figure 3B right) increased both adhesion energies in the dark- and light-activated state substantially but the adhesion energy remained higher under blue light. Notably, the GUVs with 0.5 mol % DGS-NTA lipid significantly adhered in the dark, which is not desired for the light-guided migration. It was not possible to increase the DGS-NTA lipid and hence the Micro concentration on the GUVs further because the GUVs with higher DGS-NTA lipid significantly aggregated. On the substrate side, if the iLID density was reduced by decreasing from 100% to 10% the PEG-NTA, the GUVs no longer adhered even under long blue light illumination (Supporting Information, Figure S12). Nonetheless, the adhesion energies between the GUVs and the substrate could be tuned over 3 orders of magnitude using the blue light-triggered interaction between iLID and Micro allowing for different applications. In the context of light guided motility, we used 0.1 mol % DGS-NTA lipid and 100% PEG-NTA to immobilize Micro on the GUVs and iLID on the substrate respectively, as this combination resulted in low adhesion in the dark and significant adhesion under blue light.

Even though cell motility is thoroughly studied, there are no minimal synthetic systems that are able to reproduce this behavior. A key feature of cell motility is the dynamic asymmetry in cell adhesions, which are forming at the leading edge and disassembling at the trailing edge as the cell moves forward. To mimic this dynamic asymmetry of adhesions in a synthetic minimal cell, we used light-controlled GUV adhesion. For this purpose, we observed the GUV (0.1 mol % DGS-NTA lipid) from below at the interface between the glass substrate and the GUV (x,y direction) on a confocal microscope to see the adhesion area of the GUV on the iLID functionalized substrate and locally illuminated half of the GUVs adhesion area as well as a free region in front of it (Figure 4A,B). The illumination led to spatiotemporally controlled imbalance in adhesions; more and new adhesions formed in the illuminated

DOI: 10.1021/acs.nanolett.8b03469
Nano Lett. 2018, 18, 7268−7274

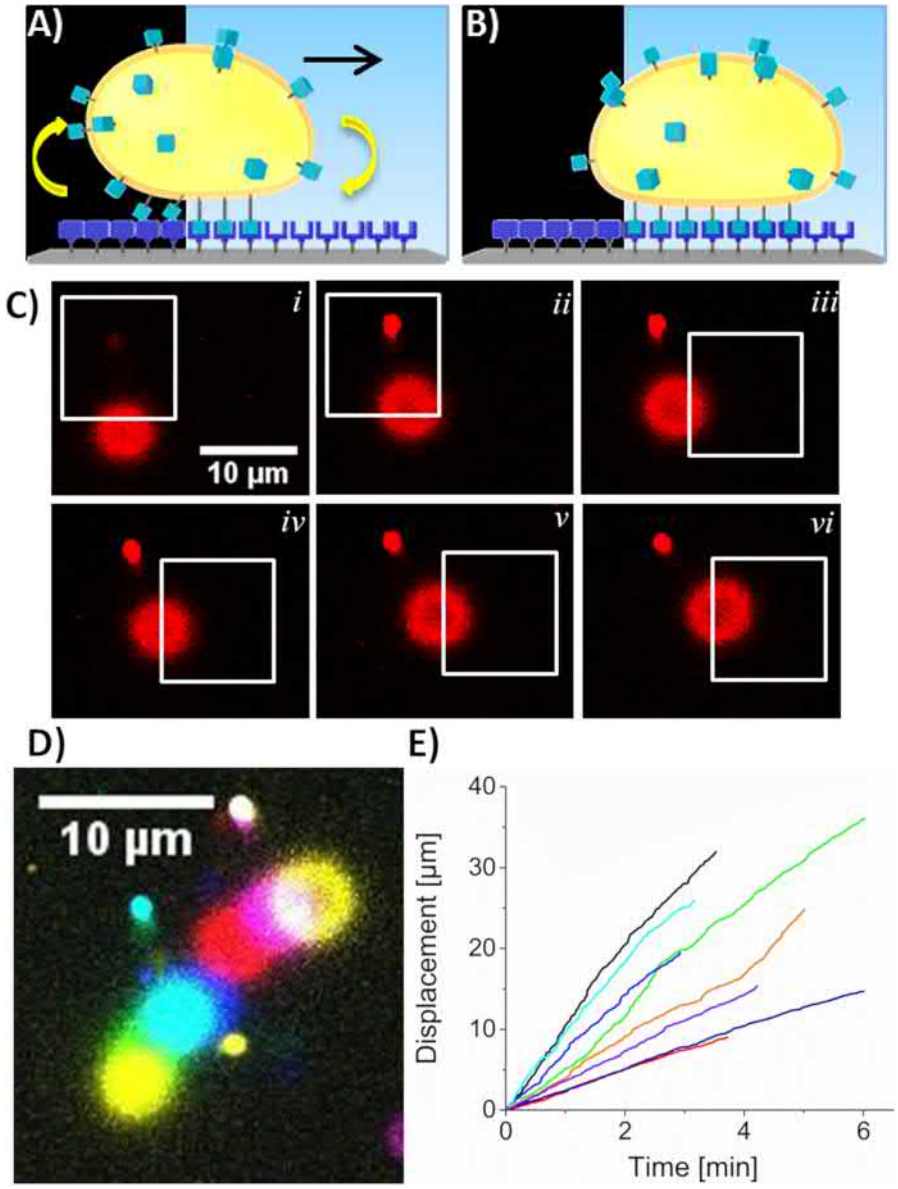

Figure 4. Light guiding. (A) Asymmetric illumination of the GUV leads to stronger adhesion in the illuminate area and weaker adhesion in the dark area. (B) This leads to migration of the GUV into the illuminated area. (C) Fluorescence microscopy images (*x,y* scans at the substrates surface $z = 0$) of a GUV (about 20 μm in diameter) from below at the adhesion site to the substrate as it moves into the blue illuminated area (shown as white square). (D) Overlay of the GUV at every illumination step (1 step about 1 min) to show GUV movement over time. (E) Displacement of GUVs versus time. Eight different GUV traces were analyzed.

half of the GUV compared to the half in the dark, where adhesions disassembled. Consequently, the GUV moved into the illuminated region, formed new adhesions in the illuminated area of the substrate, and detached from the dark part of the substrate (Figure 4 C,D, Supporting Information, Movie S1 and S2, Figure S13). Further, if the illuminated area was moved again so that only half of the GUV resides in it, the GUV followed and displaced into the new illumination area. This process could be repeated 3−7 times and the GUV could be guided over longer distances. This was also possible in multiple circuits like around a corner or back and forth (Supporting Information, Figures S14 and S15, Movie S3). In addition to the light-triggered asymmetry in adhesions, it was also essential to use deflated GUVs during light guided motility, so that the adhesion area of the GUV was large enough (about 5 μm radius) to be able to partially illuminate the GUV and to create a significant imbalance in adhesions in space and time. Moreover, the fluctuations and excess membrane in the deflated GUV might be a compensation for protrusions observed during cell motility. During light guiding, we observed cases of visible membrane shedding and also a trail of membrane (Supporting Information, Figure S16). This loss of membrane is probably the reason why GUVs can be guided over only a couple of steps and not indefinitely. Although the speed of the GUVs depended on many factors including the size of the adhesion side, the GUV size, and the membrane tension, the average speed of eight representative GUVs was 4.9 μm/min (Figure 4E). This speed is reasonably fast and is comparable to a fast moving mammalian cell.[17]

Overall, we mimic cell motility in a minimal synthetic cell, assembled from molecular components. To achieve this, we dynamically and reversibly control the adhesion of a GUV to a

DOI: 10.1021/acs.nanolett.8b03469
Nano Lett. 2018, 18, 7268−7274

substrate in space and time using the light-dependent interaction between the proteins iLID and Micro. This makes it possible to guide the migration of a GUV with light by forming new adhesions at the front of a GUV through local illumination and disassembling adhesions at the back placed in the dark. The provided examples show that it is sufficient to reproduce the dynamic and spatiotemporally controlled asymmetry in adhesions between the front and the back of a migrating cell to move cell-sized objects. In the cell, this requires complex molecular machinery but in a minimal synthetic cell this can be achieved with photoswitchable adhesions.

■ ASSOCIATED CONTENT

Supporting Information

The Supporting Information is available free of charge on the ACS Publications website at DOI: 10.1021/acs.nanolett.8b03469.

Experimental methods, thermodynamic and kinetic characterization, controls and additional examples (PDF)

Example of light-guided migration of the GUVs (AVI)

Example of light-guided migration of the GUVs (AVI)

Example of light-guided migration of the GUVs (AVI)

■ AUTHOR INFORMATION

Corresponding Author

*E-mail: wegners@mpip-mainz.mpg.de.

ORCID

Seraphine V. Wegner: 0000-0002-9072-0858

Author Contributions

S.M.B. and J.S. contributed equally.

Notes

The authors declare no competing financial interest.

■ ACKNOWLEDGMENTS

This work is part of the MaxSynBio consortium, which is jointly funded by the Federal Ministry of Education and Research (BMBF) of Germany (FKZ 031A359L) and the Max Planck Society (MPG). The pQE-80L iLID (C530M) (Addgene plasmid #60408) and pQE-80L MBP-SspB Micro (Addgene plasmid #6041ß) plasmids were gifts from Brian Kuhlman. Our thanks go to Stefan Schumacher for the illustrations.

■ REFERENCES

(1) Maiuri, P.; Rupprecht, J. F.; Wieser, S.; Ruprecht, V.; Benichou, O.; Carpi, N.; Coppey, M.; De Beco, S.; Gov, N.; Heisenberg, C. P.; Lage Crespo, C.; Lautenschlaeger, F.; Le Berre, M.; Lennon-Dumenil, A. M.; Raab, M.; Thiam, H. R.; Piel, M.; Sixt, M.; Voituriez, R. Actin flows mediate a universal coupling between cell speed and cell persistence. *Cell* **2015**, *161* (2), 374−86.

(2) Siton-Mendelson, O.; Bernheim-Groswasser, A. Toward the reconstitution of synthetic cell motility. *Cell Adh. Migr.* **2016**, *10* (5), 461−474.

(3) Smith, A. S.; Seifert, U. Vesicles as a model for controlled (de-) adhesion of cells: a thermodynamic approach. *Soft Matter* **2007**, *3* (3), 275−289.

(4) Fenz, S. F.; Sengupta, K. Giant vesicles as cell models. *Integr. Biol.* **2012**, *4* (9), 982−95.

(5) Tsai, F. C.; Stuhrmann, B.; Koenderink, G. H. Encapsulation of active cytoskeletal protein networks in cell-sized liposomes. *Langmuir* **2011**, *27* (16), 10061−71.

(6) Heuvingh, J.; Franco, M.; Chavrier, P.; Sykes, C. ARF1-mediated actin polymerization produces movement of artificial vesicles. *Proc. Natl. Acad. Sci. U. S. A.* **2007**, *104* (43), 16928−33.

(7) Hoesli, C. A.; Garnier, A.; Juneau, P. M.; Chevallier, P.; Duchesne, C.; Laroche, G. A fluorophore-tagged RGD peptide to control endothelial cell adhesion to micropatterned surfaces. *Biomaterials* **2014**, *35* (3), 879−90.

(8) Marchi-Artzner, V.; Lorz, B.; Gosse, C.; Jullien, L.; Merkel, R.; Kessler, H.; Sackmann, E. Adhesion of Arg-Gly-Asp (RGD) peptide vesicles onto an integrin surface: Visualization of the segregation of RGD ligands into the adhesion plaques by fluorescence. *Langmuir* **2003**, *19* (3), 835−841.

(9) Frohnmayer, J. P.; Bruggemann, D.; Eberhard, C.; Neubauer, S.; Mollenhauer, C.; Boehm, H.; Kessler, H.; Geiger, B.; Spatz, J. P. Minimal synthetic cells to study integrin-mediated adhesion. *Angew. Chem., Int. Ed.* **2015**, *54* (42), 12472−8.

(10) Gaul, V.; Lopez, S. G.; Lentz, B. R.; Moran, N.; Forster, R. J.; Keyes, T. E. The lateral diffusion and fibrinogen induced clustering of platelet integrin alphaIIbbeta3 reconstituted into physiologically mimetic GUVs. *Integr. Biol.* **2015**, *7* (4), 402−11.

(11) Streicher, P.; Nassoy, P.; Barmann, M.; Dif, A.; Marchi-Artzner, V.; Brochard-Wyart, F.; Spatz, J.; Bassereau, P. Integrin reconstituted in GUVs: a biomimetic system to study initial steps of cell spreading. *Biochim. Biophys. Acta, Biomembr.* **2009**, *1788* (10), 2291−300.

(12) Anamelechi, C. C.; Clermont, E. E.; Brown, M. A.; Truskey, G. A.; Reichert, W. M. Streptavidin binding and endothelial cell adhesion to biotinylated fibronectin. *Langmuir* **2007**, *23* (25), 12583−8.

(13) Fenz, S. F.; Merkel, R.; Sengupta, K. Diffusion and intermembrane distance: case study of avidin and E-cadherin mediated adhesion. *Langmuir* **2009**, *25* (2), 1074−85.

(14) Villringer, S.; Madl, J.; Sych, T.; Manner, C.; Imberty, A.; Romer, W. Lectin-mediated protocell crosslinking to mimic cell-cell junctions and adhesion. *Sci. Rep.* **2018**, *8* (1), 1932.

(15) Cardoso Dos Santos, M.; Vezy, C.; Jaffiol, R. Nanoscale characterization of vesicle adhesion by normalized total internal reflection fluorescence microscopy. *Biochim. Biophys. Acta, Biomembr.* **2016**, *1858* (6), 1244−53.

(16) Steinkuhler, J.; Agudo-Canalejo, J.; Lipowsky, R.; Dimova, R. Modulating Vesicle Adhesion by Electric Fields. *Biophys. J.* **2016**, *111* (7), 1454−1464.

(17) Maiuri, P.; Terriac, E.; Paul-Gilloteaux, P.; Vignaud, T.; McNally, K.; Onuffer, J.; Thorn, K.; Nguyen, P. A.; Georgoulia, N.; Soong, D.; Jayo, A.; Beil, N.; Beneke, J.; Lim, J. C.; Sim, C. P.; Chu, Y. S.; participants, W. C. R.; Jimenez-Dalmaroni, A.; Joanny, J. F.; Thiery, J. P.; Erfle, H.; Parsons, M.; Mitchison, T. J.; Lim, W. A.; Lennon-Dumenil, A. M.; Piel, M.; Thery, M. The first World Cell Race. *Curr. Biol.* **2012**, *22* (17), R673−5.

(18) Bartelt, S. M.; Chervyachkova, E.; Steinkuhler, J.; Ricken, J.; Wieneke, R.; Tampe, R.; Dimova, R.; Wegner, S. V. Dynamic blue light-switchable protein patterns on giant unilamellar vesicles. *Chem. Commun.* **2018**, *54* (8), 948−951.

(19) Zimmerman, S. P.; Hallett, R. A.; Bourke, A. M.; Bear, J. E.; Kennedy, M. J.; Kuhlman, B. Tuning the Binding Affinities and Reversion Kinetics of a Light Inducible Dimer Allows Control of Transmembrane Protein Localization. *Biochemistry* **2016**, *55* (37), 5264−71.

(20) Yüz, S. G.; Ricken, J.; Wegner, S. V. Independent Control over Multiple Cell Types in Space and Time Using Orthogonal Blue and Red Light Switchable Cell Interactions. *Adv. Sci.* **2018**, *5* (8), 1800446.

(21) Chen, F.; Wegner, S. V. Blue Light Switchable Bacterial Adhesion as a Key Step toward the Design of Biofilms. *ACS Synth. Biol.* **2017**, *6* (12), 2170−2174.

(22) Guntas, G.; Hallett, R. A.; Zimmerman, S. P.; Williams, T.; Yumerefendi, H.; Bear, J. E.; Kuhlman, B. Engineering an improved light-induced dimer (iLID) for controlling the localization and activity of signaling proteins. *Proc. Natl. Acad. Sci. U. S. A.* **2015**, *112* (1), 112−7.

DOI: 10.1021/acs.nanolett.8b03469
Nano Lett. 2018, 18, 7268−7274

(23) Schenk, F. C.; Boehm, H.; Spatz, J. P.; Wegner, S. V. Dual-functionalized nanostructured biointerfaces by click chemistry. *Langmuir* **2014**, *30* (23), 6897−905.
(24) Seifert, U.; Lipowsky, R. Adhesion of vesicles. *Phys. Rev. A: At., Mol., Opt. Phys.* **1990**, *42* (8), 4768−4771.
(25) Georgiev, V. N.; Grafmüller, A.; Bléger, D.; Hecht, S.; Kunstmann, S.; Barbirz, S.; Lipowsky, R.; Dimova, R. Area Increase and Budding in Giant Vesicles Triggered by Light: Behind the Scene. *Adv. Sci.* **2018**, *5* (8), 1800432.
(26) Hudson, S. V.; Dolin, C. E.; Poole, L. G.; Massey, V. L.; Wilkey, D.; Beier, J. I.; Merchant, M. L.; Frieboes, H. B.; Arteel, G. E. Modeling the Kinetics of Integrin Receptor Binding to Hepatic Extracellular Matrix Proteins. *Sci. Rep.* **2017**, *7*, 12444.
(27) Takagi, J.; Petre, B. M.; Walz, T.; Springer, T. A. Global conformational rearrangements in integrin extracellular domains in outside-in and inside-out signaling. *Cell* **2002**, *110* (5), 599−611.
(28) Dimova, R. Recent developments in the field of bending rigidity measurements on membranes. *Adv. Colloid Interface Sci.* **2014**, *208*, 225−34.
(29) Tordeux, C.; Fournier, J. B.; Galatola, P. Analytical characterization of adhering vesicles. *Phys. Rev. E: Stat. Phys., Plasmas, Fluids, Relat. Interdiscip. Top.* **2002**, *65*, 041912.
(30) Steinkuhler, J.; Rozycki, B.; Alvey, C.; Lipowsky, R.; Weikl, T. R.; Dimova, R.; Discher, D. E. Membrane fluctuations and acidosis regulate cooperative binding of "marker of self" CD47 with macrophage checkpoint receptor SIRPalpha. *J. Cell Sci.* **2019**, *4*, jcs216770.
(31) Weikl, T. R.; Asfaw, M.; Krobath, H.; Rózycki, B.; Lipowsky, R. Adhesion of membranes via receptor−ligand complexes: Domain formation, binding cooperativity, and active processes. *Soft Matter* **2009**, *5* (17), 3213.

DOI: 10.1021/acs.nanolett.8b03469
Nano Lett. 2018, 18, 7268−7274

Supporting Information

Light guided motility of a minimal synthetic cell

Solveig M. Bartelt,[†‡] Jan Steinkühler,[†§] Rumiana Dimova[§] and Seraphine V. Wegner[‡*]

[‡] *Max Planck Institute for Polymer Research, Ackermannweg 10, 55128 Mainz, Germany*
§ Theory and Bio-Systems, Max Planck Institute of Colloids and Interfaces, Science Park Golm, 14424 Potsdam, Germany

[†] These authors contributed equally to the work.

*To whom correspondence should be addressed
Email: wegners@mpip-mainz.mpg.de

Experimental Methods

Protein expression

The plasmids pQE-80L iLID (C530M) and pQE-80L MBP-SspB R73Q Micro were gifts from Brian Kuhlman (Addgene # 60408 and # 60409, respectively). pQE-80L iLID (C530M) expresses iLID with an N-terminal His6-tag and pQE-80L MBP-SspB R73Q Micro expresses Micro with N-terminal His6-MBP-TEV tag (His6-MBP-TEV-Micro).). mOrange-GGS was a gift from Spatz Lab. The mOrange-GGS was inserted into pQE-80L MBP-SspB R73Q Micro after the BamH1 cutting site to yield His6-MBP-TEV-mOrange-Micro. His6-tagged TEV protease originated from the Wombacher Lab and was kindly provided as a glycerol stock of *E. coli* BL21 (DE3) co-transformed with pLysS (chloramphenicol) and pET N_TEV234 (kanamycin) plasmids.

A standard protocol was used to recombinantly express in *E. coli* and purify all proteins. In brief, 1 L LB medium with 50 mg/L antibiotic was inoculated with 10 mL of the respected overnight culture. The bacteria were allowed to grow at 37 °C and 200 rpm till an OD_{600}=0.6-0.8 was reached. To induce protein expression 500 µM IPTG was added and the culture allowed to grow at 16 °C overnight (except for TEV-Protease, which was grown at room temperature overnight). The harvested bacteria were resuspended in 20 mL of Buffer A (50 mM Tris, 300 mM NaCl, pH 7.4) with 100 µM PMSF (in methanol) on ice. After sonication at 0 °C (50% frequency, 40% power, 10 min) the lysate was separated from the supernatant by centrifugation (12000 rpm, 4°C, 30 min). The supernatant was consequentially purified by Ni^{2+}-NTA affinity column with ice cold elution buffer (Buffer A with 250 mM Imidazole) and

gel filtration (HiLoad 16/600 Superdex 200 pg, GE Healthcare). All proteins were stored in Buffer with the exception of His6-TEV (Buffer composition: 50 mM Tris, 400 mM NaCl, 2 mM EDTA, pH 7.4). The purity was checked by Gel electrophoresis on 12% SDS-gels and the concentration determined by UV-Vis spectral analysis.

TEV-cutting

To prevent the binding of Micro proteins to NTA-groups during the QCM-D measurement the MBP-SspB R73Q Micro was cut at the TEV cleaving site, removing the His6-tag. Therefore, the protein was incubated 50:1 with TEV-protease in a dialysis tube (3.5 kDa cut off, Spectrum Laboratories, Inc.) in TEV reaction buffer (50 mM Tris, 500 nM EDTA, pH=8, 1 mM DTT) over night at 4 °C at low stirring speed. The cut protein was purified by His-trap-column, as the protease and uncut protein would bind to the column through His-tags, while the cutMicro was collected as flow through. The result was verified by 12% SDS-PAGE. The new protein concentration was determined by UV-Vis spectral analysis.

GUV formation and functionalization

GUVs were formed using the polyvinylalcohol (PVA)-gel assisted formation as described earlier.[1] 50 µL of a 5% PVA solution in MiliQ with 100 mM sucrose was deposited on a microscopy glass slide (60 mm x 24 mm, #1.5) as a thin film. To dehydrate the PVA layer, the glass slide was kept at 50 °C for 1 h. Afterwards, 5 µL of the lipid solution consisting of 10 mg/ml 1-Palmitoyl-2-oleoylphosphatidylcholine (POPC), 10 mol% 1-palmitoyl-2-oleoyl-sn-glycero-3-phospho-(1'-rac-glycerol) (POPG), 0.1 mol% 1,2-dioleoyl-sn-glycero-3-[(N-(5-amino-1-carboxypentyl)iminodiacetic acid) succinyl] Ni^{2+}-Salt (DGS-NTA-Ni^{2+}) and 1 mol% 1,1'-Dioctadecyl-3,3,3',3'-Tetramethylindodicarbo-cyanine (DiD) dye in chloroform (all lipids were purchased from Avanti Polar Lipids) was spread onto the PVA film and the chloroform removed by heating to 30 °C or keeping the samples in vacuum for 1 h. Then a chamber was built on the glass slide with the help of a Teflon frame (ca. 40 mm x 24 mm) and a second glass slide. Into this chamber ca 1 mL of rehydration buffer (10 mM Tris, 100 mM NaCl, pH 7.4, ~305 mOsmol) was injected. The GUVs were allowed to grow for 1 h at room temperature before they were harvested and used without further dilution. To functionalize the GUVs, they were incubated with 1 µM (final concentration) of the corresponding protein for 1 h in dark at room temperature.

Surface functionalization and passivation

Standard microscopy slides (60 mm x 24 mm, # 1.5) were functionalized with 100 % PEG-NTA as previously described using PEG-azide-3000 and NTA-alkyne.[2] To decrease the PEG-NTA density to 10 %, a nonreactive PEG2000-silane was mixed into the functionalization mixture with PEG-azide-3000 in the corresponding mol ratio. The NTA-groups were the loaded with Ni^{2+} by incubating the surfaces in 10 mM $NiCl_2$ solution for 15 min. The surfaces were thoroughly washed by placing them in two consequential buffer (10 mM Tris, 100 mM NaCl, pH 7.4) baths. Then the surfaces were incubated with 1 µM iLID solution for 30 min at room

temperature and again thoroughly washed with buffer immediately before use. The sample was always handled in the dark or under red light by a standard red 15 W LED lamp.

To passivate microscopy slides to prevent GUV bursting or absorption of protein, the slides were incubated with 3 wt% BSA solution in MilliQ for 15 min. The excess was washed with MiliQ and dried in a nitrogen stream.

Imaging of GUV adhesion

Press-to-Seal^{TM} silicon isolators were used to create a chamber between a functionalized and a passivated microscopy slide to prevent evaporation of the imaging sample. Into this chamber a drop of 10 µL of functionalized GUV solution with 10 µL buffer was introduced. For imaging, a Leica SP5 laser scanning confocal microscope with a FRAP (Fluorescence Recovery after Photobleaching) module with a 63x water objective was used. The 633 nm laser was used to image the lipid dye DiD and thus the membrane (indicated in red in microscopy pictures). In the case of membrane staining with DII the 561 nm laser was used for imaging The surface was detected by the transmission light channel and imaged in reflection with the 561 nm laser (indicated in green in microscopy pictures). For imaging the adhesion of GUVs, (x,z) cross-section (relative to the substrate in the (x,y) plane) confocal scans were obtained at varying sample heights. If not indicated otherwise, the sample was observed in the (x,z) plane and illuminated continuously with blue light (488 nm Laser) and 1 scan per ca. 2 s was acquired using 633 nm excitation light. Following illumination protocol was used: about 30 s of dark, then ca. 10 min of blue light exposure with the 488 nm laser at 10% laser intensity (1790 ± 71 nW), followed by another ca. 10 min observation without 488 nm in the dark to show reversibility. The observation was stopped when no further reversion was visible. The GUVs were always imaged at the position of maximum diameter between adhering GUV segment and the substrate. The shown pictures were scaled compared to the spherical GUVs in solution to avoid distortion of the image. To image multiple adhesions of the same GUV the same protocol was used as described above but the illumination time with the 488 nm laser and the reversion time in the dark were reduced to 5 min each. The dark/light cycle was repeated up to 4 times.

Analysis of Micro distribution over the GUV

The experiment was performed the same way as described above (imaging of GUV adhesion) with following changes. Instead of functionalizing the GUVs with Micro, His-tagged Micro-mOrange was used, making it possible to observe the Micro-mOrange distribution over the GUV in the TRITC channel on a confocal microscope. The GUVs were observed in the x,z plane at 1 scan ca. every 2 s. The GUVs were initially imaged in the dark for about 30 s and then exposed to blue light for ca. 15 min with the 488 nm laser at 10% laser intensity. The mOrange fluorescence was analysed with ImageJ software, measuring the mean intensity of fluorescence before and after adhesion at the adhesion site and the top of the GUV and subtracting the contribution of the surface reflection at the adhesion site. Effect of different Micro concentrations and cholesterol concentrations on GUV adhesion

The experiments were done as described above but following lipid compositions were used:

0.5 % DGS-NTA GUVs: 10 mg/ml 1-Palmitoyl-2-oleoylphosphatidylcholine (POPC), 10 mol% 1-palmitoyl-2-oleoyl-sn-glycero-3-phospho-(1'-rac-glycerol) (POPG), 0.5 mol% 1,2-dioleoyl-sn-glycero-3-[(N-(5-amino-1-carboxypentyl)iminodiacetic acid) succinyl] Ni^{2+}-Salt (DGS-NTA-Ni^{2+}) and 1 mol% 1,1'-Dioctadecyl-3,3,3',3'-Tetramethylindodicarbo-cyanine (Dii) dye in chloroform (all lipids were purchased from Avanti Polar Lipids)

20 % Cholesterol GUVs: 10 mg/ml 1-Palmitoyl-2-oleoylphosphatidylcholine (POPC), 10 mol% 1-palmitoyl-2-oleoyl-sn-glycero-3-phospho-(1'-rac-glycerol) (POPG), 0.1 mol% 1,2-dioleoyl-sn-glycero-3-[(N-(5-amino-1-carboxypentyl)iminodiacetic acid) succinyl] Ni^{2+}-Salt (DGS-NTA-Ni^{2+}), 20 mol% Cholesterol and 1 mol% 1,1'-Dioctadecyl-3,3,3',3'-Tetramethylindodicarbo-cyanine (DiD) dye in chloroform (all lipids were purchased from Avanti Polar Lipids)

40 % Cholesterol GUVs: 10 mg/ml 1-Palmitoyl-2-oleoylphosphatidylcholine (POPC), 10 mol% 1-palmitoyl-2-oleoyl-sn-glycero-3-phospho-(1'-rac-glycerol) (POPG), 0.1 mol% 1,2-dioleoyl-sn-glycero-3-[(N-(5-amino-1-carboxypentyl)iminodiacetic acid) succinyl] Ni^{2+}-Salt (DGS-NTA-Ni^{2+}), 40 mol% Cholesterol and 1 mol% 1,1'-Dioctadecyl-3,3,3',3'-Tetramethylindodicarbo-cyanine (DiD) dye in chloroform (all lipids were purchased from Avanti Polar Lipids)

GUV preparation and imaging of adhesion were done in the same way.

Quantification of adhesion energy

Adhesion energies were estimated from the global shape of the GUV as described in detail elsewhere[3]. Images were obtained by confocal microscopy (e.g. as shown in Figure 2B) and were corrected for optical aberrations and other distortions by calibration to spherical GUV in solution. Adhering GUV area, volume and substrate-membrane contact area were extracted from (x,z) cross-section scans by image analysis (Image J 1.52b). Using the obtained geometry parameters, adhesion energies were estimated from analytical approximations of shape equations describing adhering vesicles (method termed „First method of image analysis" in Ref. [3]). The method relies on the measurements of adhesion area and GUV area and volume. Area and volume were extracted from three dimensional reconstructions obtained by confocal microscopy (vertical cross sections). The analysis assumed axisymmetric GUV shapes and area and volume were found by integration of the vesicle contour. Because shape fluctuations lead to distortions during this analysis, up two four measurements were obtained per GUV and the median value for area and volume was used. The relation between adhesion energy W rescaled by the membrane bending rigidity κ can be expressed to a leading order in $R - R_0$ as [4]:

$$(1)\ W/\kappa \approx \frac{2}{(R-R_0)^2}\left(\frac{\cos\left(\frac{\theta_0}{2}\right)}{1+\sin\left(\frac{\theta_0}{2}\right)}\right)^2$$

where the angle θ_0 and radius R_0 only depend on the area and volume of the GUV[4]. The change in GUV adhesion energies between dark and light activated state was found by

measurement of adhesion area radius R for a given set of θ_0, R_0 values measured on an individual GUV.

Quantification of adhesion kinetics

The GUV adhesion and unbinding kinetics were quantified by the change of GUV-substrate contact area during light activation or incubation in the dark. Time-series from confocal (x,z) scans were obtained and quantification was performed by automated image analysis. Micrographs of GUV membrane signal and water-substrate interfaces were binarized individually (ImageJ 1.52b). The overlap (*co-localisation)* between the two channels was estimated by multiplication of the two binary images. Further image processing (Gaussian filtering and subsequent edge detection) was used to find an estimate of the adhesion area of the GUV at each time-point (MATLAB 2014a). The adhesion area is a measure of the change of adhesion energy as long the GUV area and volume stay approximately constant which is usually the case during the experiments, see eq. (1).

Light guiding of GUVs

To observe the GUVs the same settings imaging settings were used as described above with the following changes: The GUVs were observed in x,y-direction in the immediate vicinity of the glass substrate (z=0 position), where the adhesion area of the GUV with the glass substrate could be observed. A region of interest (ROI) was chosen such that it included ca. half of the GUV adhesion area and a vesicle-free region of similar surface area. The ROI was illuminated continuously with blue light (488 nm Laser) at 10% laser intensity (1790 ± 71 nW) and the GUV's movement was monitored by acquiring 1 scan every 2 s using 633 nm laser light excitation till the GUV stopped movement into the illuminated area. Then the ROI was adjusted such that again half of the GUV was within the ROI and the new ROI was illuminated using the same settings. Depending on the size of ROI every ROI was illuminated for ca. 1-2 min.

To analyse the speed of GUV movement, the GUV images were binarized with ImageJ and holes were filled by using the ImageJ. Subsequently, the centre of mass of the GUV was determined for each time point using the analyse particle tool in ImageJ. From the coordinates of the centre of mass the displacement was calculated for each time interval and the speed was calculated for 8 different GUVs.

QCM-D

All QCM-D experiments were performed on a Qsense Analyser E4 with either flow modules (dark state) or window modules with a standard 15 W blue LED lamp to illuminate the sample with blue light as described before [5]. The flow rate was kept at all times at 200 µL/min and in all experiments SiO_2 crystals were used.

All components were used in Buffer (10 mM Tris, 100 mM NaCl, pH 7.4) and excess was always removed by washing with an excess of Buffer. Components were washed over the crystal in the following order: 1) 1 mL of 0.1 mg/ml DOPC + 5 mol% DGS-NTA with 5 mM

$CaCl_2$ to form a supported lipid bilayer (the pump was stopped after total addition and waited till a bilayer was formed), 2) 10 mM $NiCl_2$ for 5 min to load the NTA-groups with Ni^{2+}, 3) 1 ml of 1 µM iLID (the flow was stopped until the frequency stabilized). Step by Step 1 mL cutMicro was flown at increasing concentrations (125 nM, 250 nM, 500 nM, 1 µM, 2 µM) over the crystal and the flow was stopped after every addition until the frequency had stabilized to assure complete binding. cutMicro was washed with an excess of buffer to show the unbinding behaviour of the protein. As the last step, buffer with 250 mM imidazole was flushed onto the crystal to for ca. 5 min to confirm the specific binding of iLID to the NTA head groups of the lipid bilayer.

For analysis the thickness of the resulting layers was modelled with the QTools (Bioline Scientific Inc.) software according to the standard protocol. The thermodynamic and kinetic constants can be calculated from the thickness of the film: K_d was calculated by fitting thickness with the according cutMicro concentrations to a Hill-fit with one binding site and k_{off} computed from the wash off behaviour with QTools. k_{on} was then calculated from these values as k_{on} equals k_{off} divided by K_d. The mean values were acquired from three technical replicates and the standard deviation given.

References:

(1) Weinberger, A.; Tsai, F. C.; Koenderink, G. H.; Schmidt, T. F.; Itri, R.; Meier, W.; Schmatko, T.; Schroder, A.; Marques, C., Gel-assisted formation of giant unilamellar vesicles. *Biophys J.* **2013,** *105* (1), 154-64.

(2) Chen, F.; Wegner, S. V., Blue Light Switchable Bacterial Adhesion as a Key Step toward the Design of Biofilms. *ACS Synth. Biol.* **2017,** *6* (12), 2170-2174.

(3) Steinkuhler, J.; Agudo-Canalejo, J.; Lipowsky, R.; Dimova, R., Modulating Vesicle Adhesion by Electric Fields. *Biophys J.* **2016,** *111* (7), 1454-1464.

(4) Tordeux, C.; Fournier, J. B.; Galatola, P., Analytical characterization of adhering vesicles. *Phys Rev.* **2002,** *65*, 041912.

(5) Bartelt, S. M.; Chervyachkova, E.; Steinkuhler, J.; Ricken, J.; Wieneke, R.; Tampe, R.; Dimova, R.; Wegner, S. V., Dynamic blue light-switchable protein patterns on giant unilamellar vesicles. *Chem. Comm.* **2018,** *54* (8), 948-951.

(6) Hudson, S. V.; Dolin, C. E.; Poole, L. G.; Massey, V. L.; Wilkey, D.; Beier, J. I.; Merchant, M. L.; Frieboes, H. B.; Arteel, G. E., Modeling the Kinetics of Integrin Receptor Binding to Hepatic Extracellular Matrix Proteins. *Sci. Rep.* **2017,** *7*.

(7) Litvinov, R. I.; Mekler, A.; Shuman, H.; Bennett, J. S.; Barsegov, V.; Weisel, J. W., Resolving two-dimensional kinetics of the integrin alphaIIbbeta3-fibrinogen interactions using binding-unbinding correlation spectroscopy. *J Biol. Chem.* **2012,** *287* (42), 35275-85.

(8) Germer, M.; Kanse, S. M.; Kirkegaard, T.; Kjoller, L.; Felding-Habermann, B.; Goodman, S.; Preissner, K. T., Kinetic analysis of integrin-dependent cell adhesion on vitronectin--the inhibitory potential of plasminogen activator inhibitor-1 and RGD peptides. *Eur. J. Biochem.* **1998,** *253* (3), 669-74.

(9) Kim, J. K.; Xu, Y.; Xu, X.; Keene, D. R.; Gurusiddappa, S.; Liang, X.; Wary, K. K.; Hook, M., A novel binding site in collagen type III for integrins alpha1beta1 and alpha2beta1. *J. Biol. Chem.* **2005,** *280* (37), 32512-20.

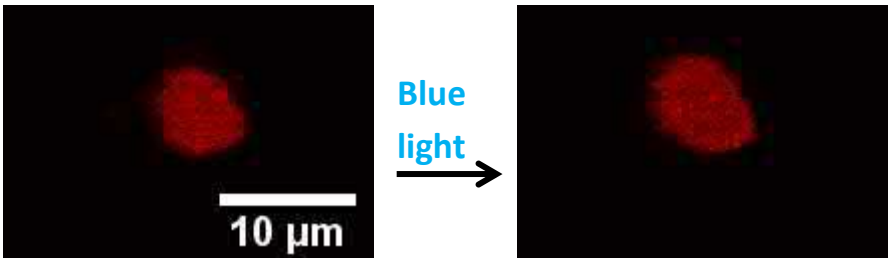

Figure S1. Adhesion area increase of a GUV after 10 min irradiation with blue light. Adhesion area was detected from x,y-scans at the surface of the substrate. A clear increase in adhesion area was visible upon blue light illumination.

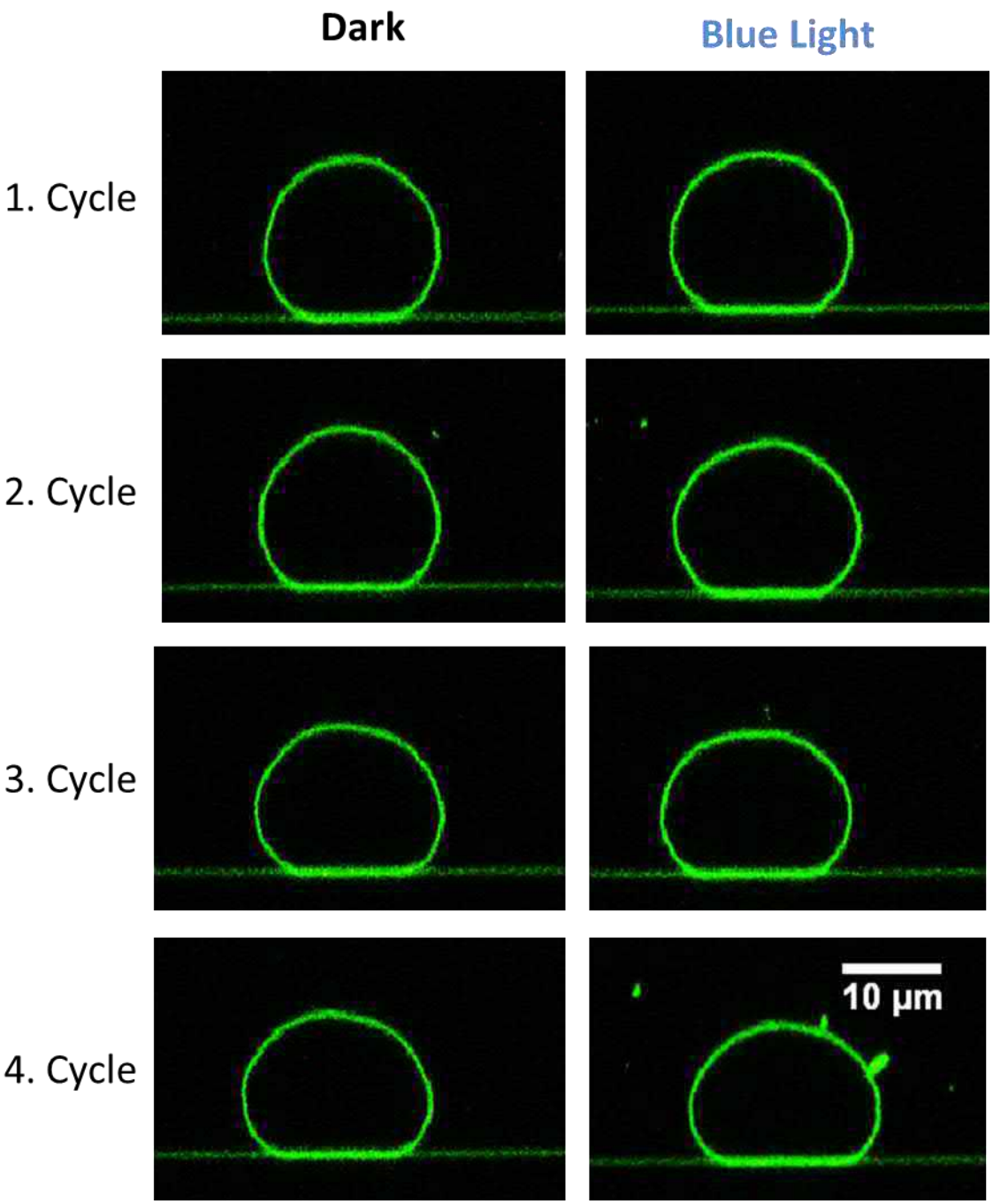

Figure S2. Adhesion of a GUV over multiple dark/blue light cycles. Images of the GUV were acquired in the x,z plane after each 5 min. period in the dark and 5 min. under blue light over 4 cycles. The adhesion site of the GUV increased after each blue light exposure and decreased each time illumination with blue light was stopped.

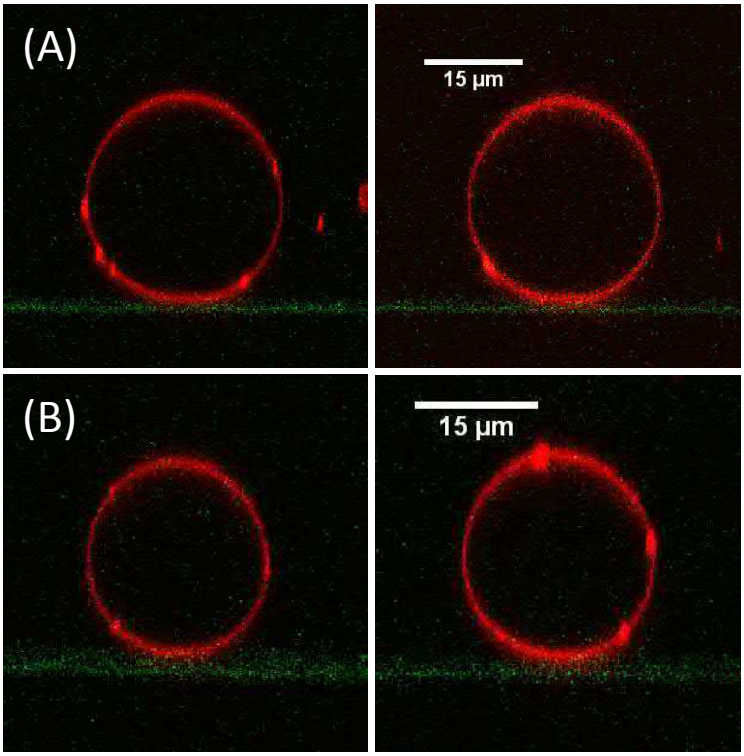

Figure S3. Negative controls of adhesion. Images of the GUV were acquired in the x,z plane. (A) iLID-functionalized substrate (green) with Micro functionalized GUVs (red) observed over a 10 min period in the dark; before (left image) and after 10 min (right). No change in adhesion was observed. (B) mOrange functionalized substrate (green) with Micro functionalized GUVs (red) under blue light illumination observed over 10 min; before (left) and after 10 min (right). No change in adhesion was observed.

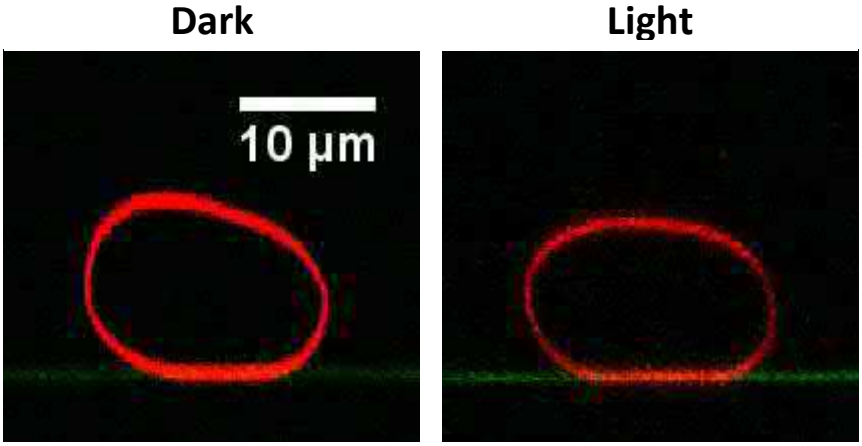

Figure S4 Images of an iLID-functionalized GUV on a Micro functionalized substrate were acquired in the x,z plane before and after 10 min blue light illumination. Swapping the positions of the proteins resulted in similar blue light dependent GUV adhesion to the substrate as observed through increased adhesion site and GUV deformation.

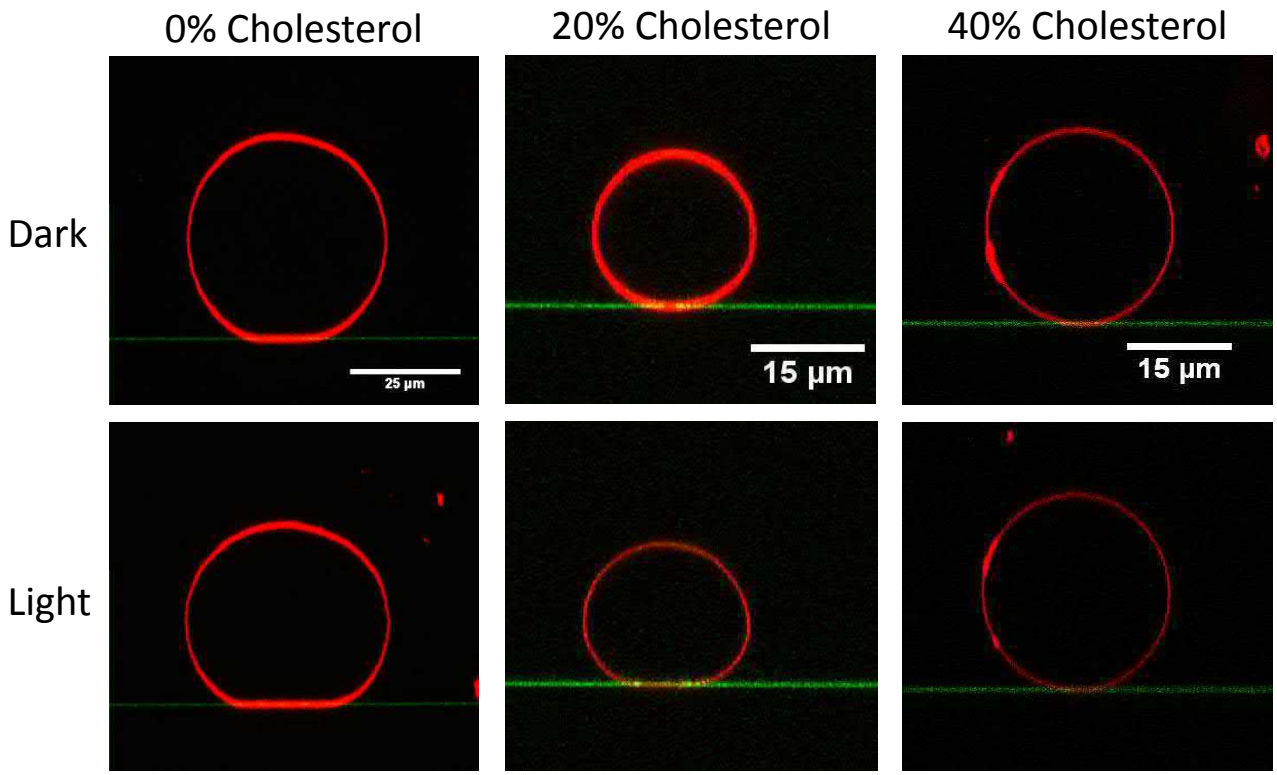

Figure S5 Effect of GUV membrane stiffness induced by different cholesterol concentrations (0-40 %) on the adhesion of deflated GUVs. Images of the GUVs in the x,z-plane were acquired in the dark and after 10 min blue light illumination. The GUV without cholesterol showed clear adhesion under blue light in form of deformation, increase in adhesion site and clear change in apparent adhesion angle, showing that membrane is clearly attached to the surface. The GUV with 20% cholesterol also changed its morphology upon blue light illumination, but the deformation was less pronounced and the GUV contact curvature between membrane and substrate stayed above the optical resolution. The GUV with 40% cholesterol did not change its shape upon light illumination. These differences in adhesion showed that membrane flexibility and fluidity are important for light dependent adhesion. High concentrations of cholesterol impede the flexibility of the membrane reducing the deformation due to adhesion to a degree that adhesion is below the optical resolution.

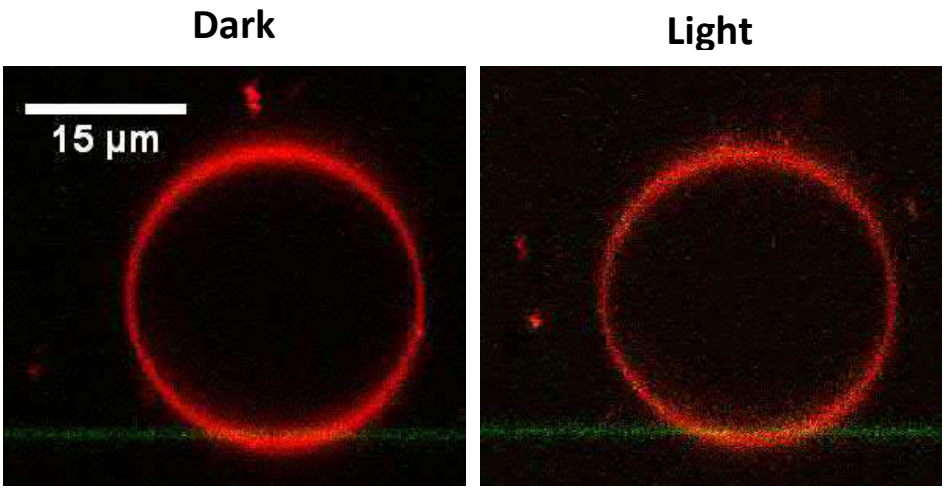

Figure S6 Adhesion of a fully inflated GUV in dark and after 10 min light exposure. Images were acquired in the x,z plane. Through the stiffness of the fully inflated GUV and the lack of excess membrane there were no obvious signs of adhesion like deformation and only a very small increase in adhesion site, if at all.

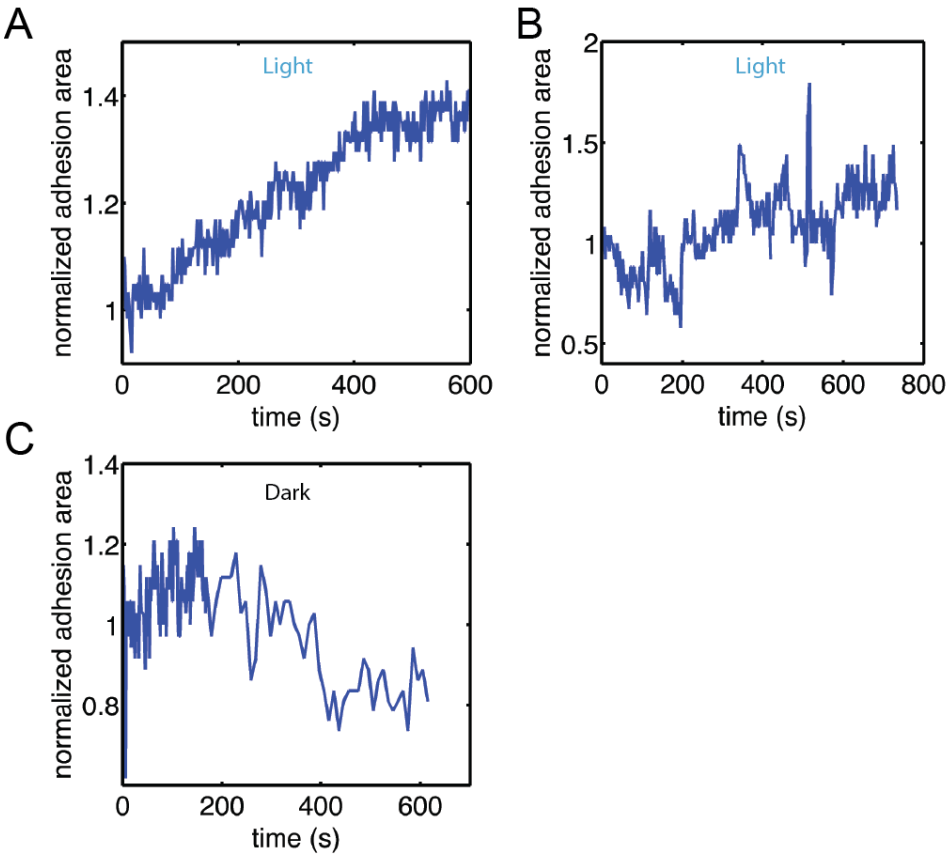

Figure S7 Additional examples of light induced (A) adhesion and (C) reversion kineticsof the adhered GUVs. Apparent noise in the normalized adhesion area traces is partly due to unprecise quantification of the adhesion segments but also reflects movement or membrane fluctuations of the vesicles themselves.

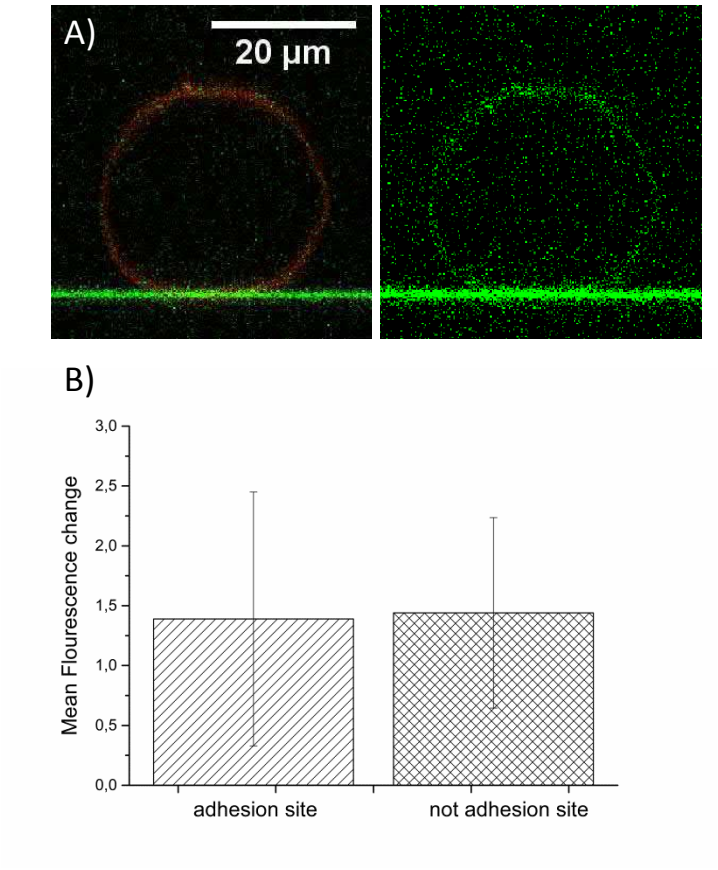

Figure S8. mOrange-Micro distribution over on a adhered GUV. A) Fluorescence image of the lipid membrane (red) and the mOrange (green of an adhered vesicle) were acquired in the x,z plane. The mOrange signal was homogeneously distributed over the whole GUV. B) mOrange fluorescent intensity analysis of six GUVs at the adhesion site and the top of the GUV (not adhesion site). The contribution of from the reflection at the substrate was subtracted. The change in fluorescence before and after adhesion is expectedly small. The error bars, which are the standard deviation, indicate that change in fluorescence intensity before and after blue light activation were not significantly different in different parts of the GUVs. Hence, within the sensitivity of this method the adhesion did not result in enrichment of Micro at the adhesion site.

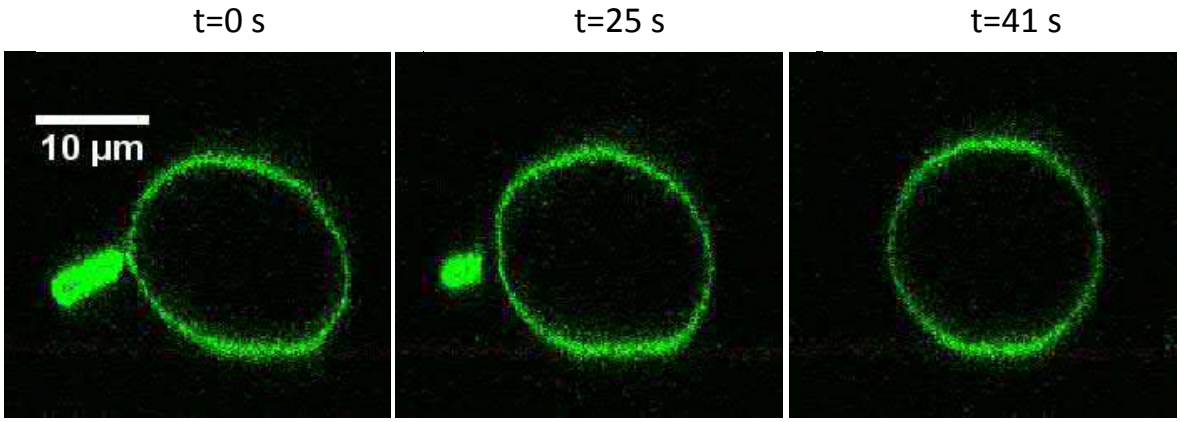

Figure S9. Fluorescence images in the x,z plane, of membrane shedding of a GUV adhered under blue light after placing back in the dark. During reversion of the GUV adhesions in the dark in some cases (ca. 30-40 % of observed GUVs) membrane shedding was observed in the form of bud release accompanying the GUV stabilization and the detachment of the GUV over a timespan of seconds to minutes.

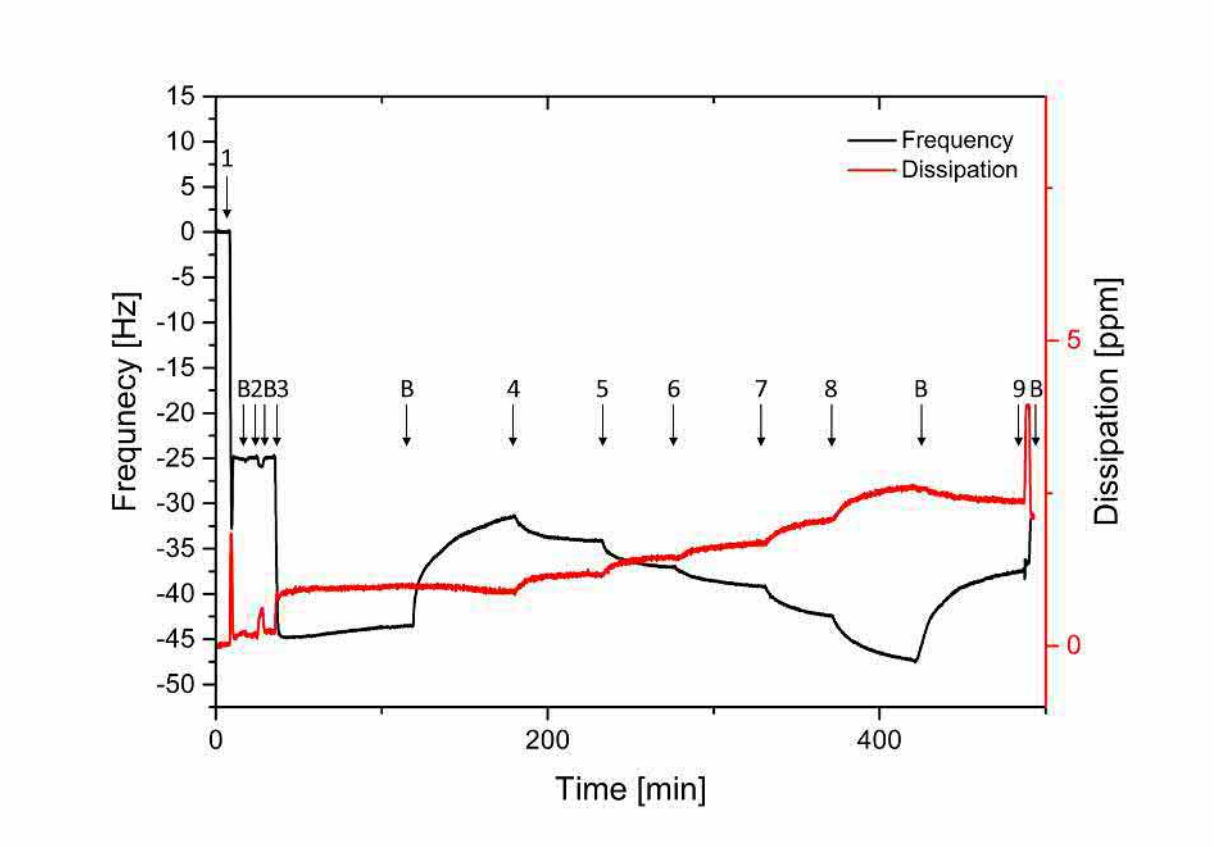

Figure S10. Exemplary changes of frequency and dissipation (7th overtone) in QCM-D measurements. Arrows indicate the start of addition of the following components in buffer (150 mM NaCl, 10 mM Tris, pH 7.4). 1) 10 mg/ml Lipids (DOPC + 5 mol% DGS-NTA) with 5 mM $CaCl_2$, 2) 10 mM $NiCl_2$, 3) 1 µM iLID, 4) 125 nM cutMicro, 5) 250 nM cutMicro, 6) 500 nM cutMicro, 7) 1 µM cutMicro, 8) 2 µM cutMicro, 9) 250 mM imidazole. 'B' indicates washing steps with buffer.

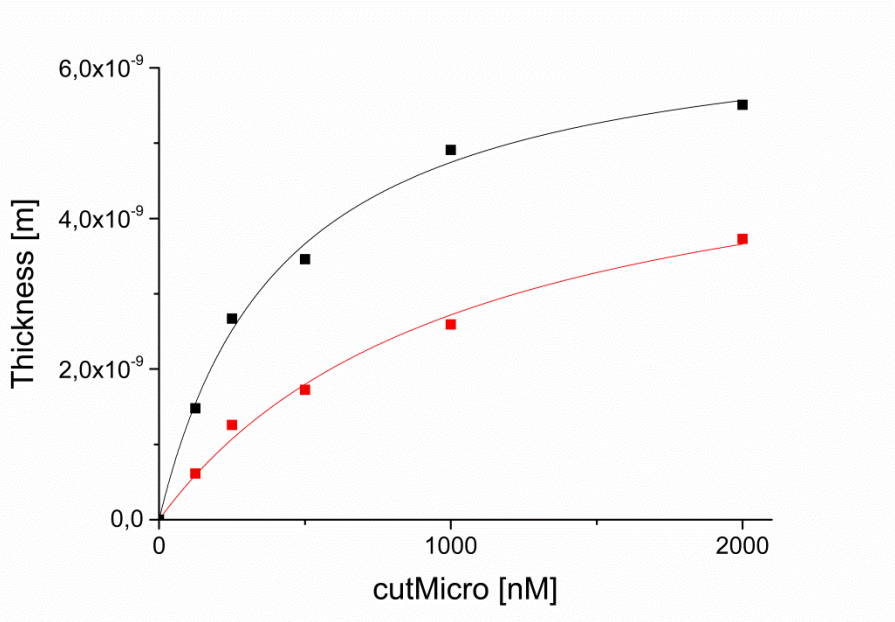

Figure S11. Film thickness as fitted to the QCMD measurements vs. cutMicro concentrations in dark (red) and under blue light illumination (black). The curves show Hill-fits.

Table S1. Thermodynamic and kinetic constants of the iLID/Micro protein pair compared to natural adhesion proteins.

Constants	Blue light	Dark	αvβ3-fibrinogen [6-7]	αvβ3-vitronectin [6, 8]	α1β1-collagen [6, 9]
K_d [µM]	0.95 ± 0.47	2.63 ± 1.78	0.055	0.12	0.023
k_{off} [s^{-1}]	$1.1 \times 10^{-3} \pm 2.2 \times 10^{-4}$	$8.5 \times 10^{-4} \pm 4.4 \times 10^{-4}$	2.8×10^{-3}	9.2×10^{-4}	1.3×10^{-3}
k_{on} [$M^{-1}s^{-1}$]	$1.2 \times 10^{3} \pm 0.2 \times 10^{3}$	$3.2 \times 10^{2} \pm 0.2 \times 10^{3}$	5.1×10^{4}	7.9×10^{3}	5.6×10^{4}

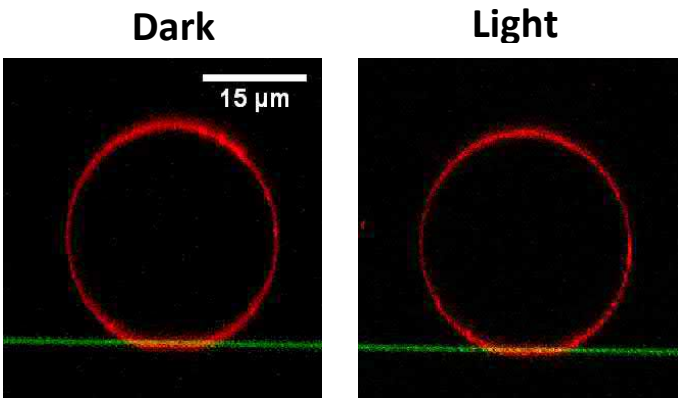

Figure S12. Adhesion of a Micro-functionalized GUV (0.1 % DGS-NTA) on a 10 % PEG-NTA substrate functionalized with iLID before and after 10 min blue light illumination. Images were acquired in the x,z plane. The GUV did not significantly adhere under blue light to the substrate with low iLID functionalization density.

A) **B)**

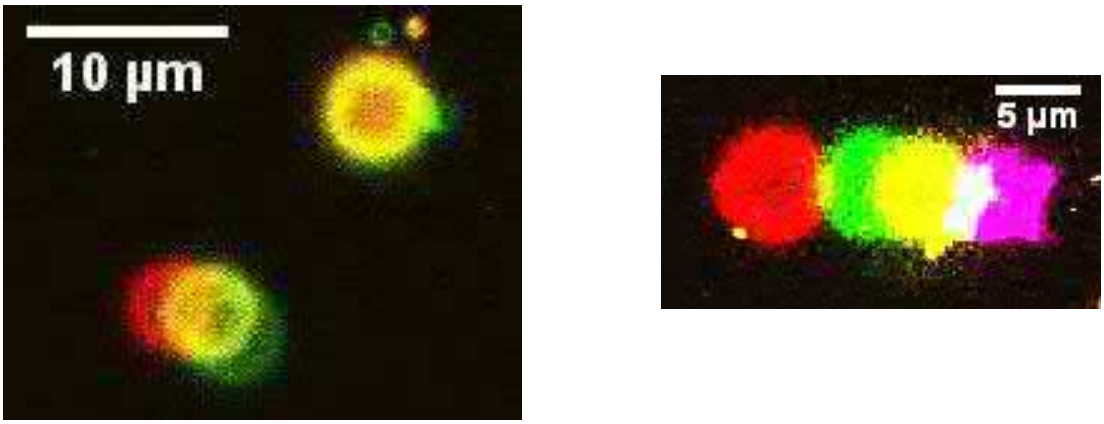

Figure S13. Light guided of GUVs. A) Overlay of GUV adhesion sites at different time points. The different colors correspond to different time points (red start, green end) spaced by ca 1.5 min. The movement of the GUV in the bottom-left corner was guided by illuminating half of the GUV, while the GUV in the upper-right corner was not exposed to light and thus did not move (Movie S1). B) Another example of a light guided GUV by illuminating half of the GUV and moving the illumination region as the GUV moves forward.

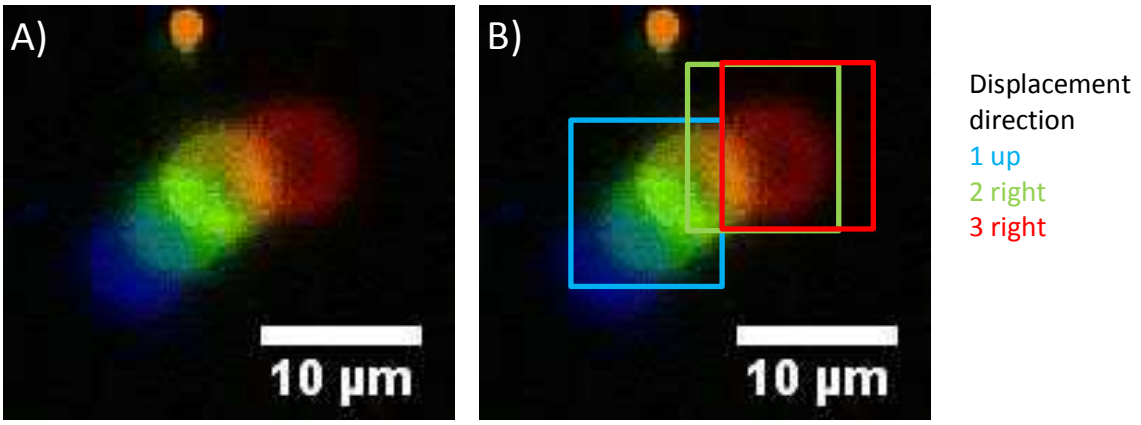

Figure S14. Light guiding of a GUV around a corner. A) Overlay of movement of GUV at different time points and with different guiding directions around a corner. B) Illumination areas indicated at different steps and the intended guiding direction. Blue is the initial illumination area moving the GUV upwards. Green indicates the 2nd und red the 3rd step guiding the GUV to the right.

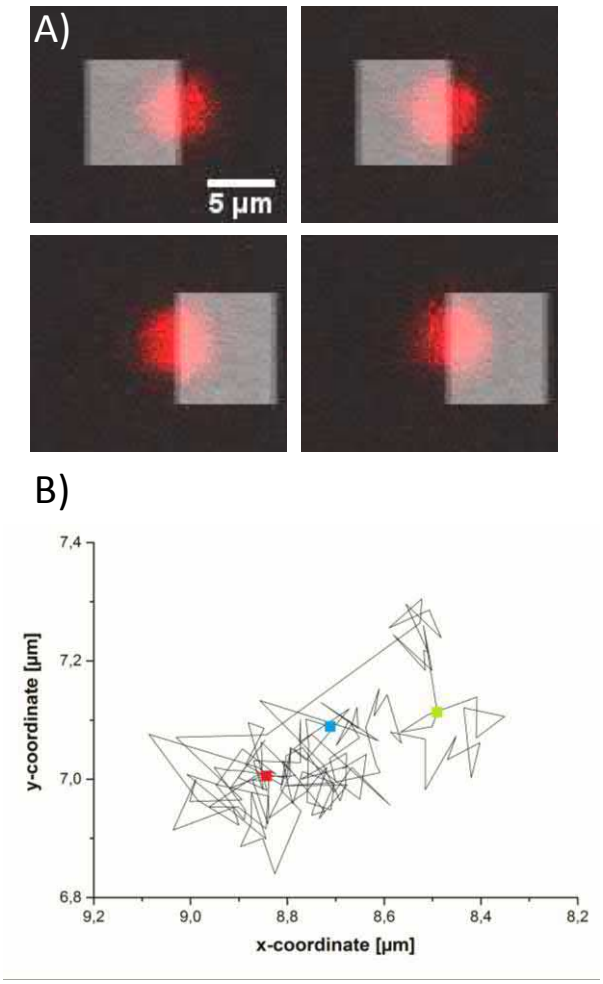

Figure S15. Back and forth light guiding of a GUV. A) The light areas show the illuminated areas and the movement of the red GUV into the illuminated area. Number 1-4 indicate timely sequence of events. (Movie S3). B) Direction map of GUV movement was generated by following the center of the GUV. Blue indicates the starting point, red indicates endpoint of the illumination to the left and green indicates endpoint of illumination to the right.

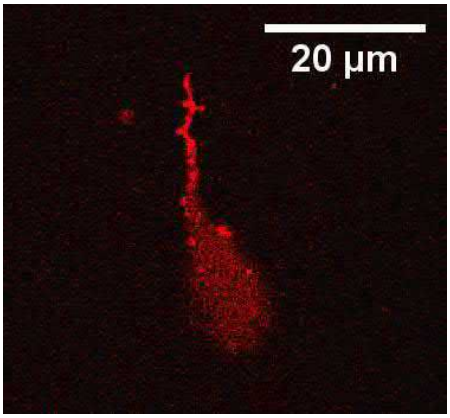

Figure S16. Membrane shedding during light guiding of a GUV. Some GUVs produce membrane tails during movement.